the acidity of Zn^{II}. (vi) In carboxypeptidase A, Zn^{II} is coordinated with two N (from two histidines, His(69), His(196)) and one anionic O^- (from the carboxylate of Glu(72)).[38] These ligands would not make the Zn^{II} ion acidic enough to produce a Zn^{II}–OH^- species from Zn^{II}–OH_2. Only with the cooperation of COO^- (Glu(270)) can the Zn^{II}-bound water come to act as a reactive nucleophile.[39] Our present experimental data for this model are compatible with this interpretation. In the recent ab initio calculation, Bertini et al. found a similar acidity-weakening effect by anionic ligands ($HCOO^-$ and CH_3S^-).[40] (vii) Finally, in actual Zn^{II} enzymes, there might be special environmental devices for the Zn^{II}–OH^- moiety to work as a nucleophile. Otherwise, Zn^{II}–OH^- might merely act as a base to dissociate a proton from the nearby peptides.

(38) Rees, D. C.; Lewis, M.; Honzatko, R. B.; Lipscomb, W. N.; Hardman, K. D. *Proc. Natl. Acad. Sci U.S.A.* **1981**, *78*, 3408–3412.
(39) Christianson, D. W.; Lipscomb, W. N. *Acc. Chem. Res.* **1989**, *22*, 62.
(40) Bertini, I.; Luchinat, C.; Rosi, M.; Sgamellotti, A.; Tarantelli, F. *Inorg. Chem.* **1990**, *29*, 1460.

Registry No. **3**, 85828-26-8; **5**, 108643-56-7; **6**, 129620-89-9; **8**, 129620-90-2; **10**, 91328-02-8; (**14**)ClO_4·$2H_2O$, 129648-16-4; (**15**)$(ClO_4)_2$·$2H_2O$, 129648-18-6; (**16**)ClO_4·H_2O, 129620-92-4; (**16**)ClO_4·$3H_2O$, 129648-19-7; (**17**)$(ClO_4)_2$·H_2O, 129620-94-6; (**18**)ClO_4·H_2O, 129620-96-8; (**19**)ClO_4·$2H_2O$, 129620-98-0; (**20**)·H_2O, 129620-99-1; (**22**)ClO_4·$2H_2O$, 129621-01-8; (**23**)·H_2O, 129621-02-9; (**26**)$(ClO_4)_2$·$2H_2O$, 129621-04-1; (**27**)ClO_4·H_2O, 129621-06-3; (**28**)$(ClO_4)_2$·$2H_2O$, 129621-08-5; (**29**)ClO_4·H_2O, 129621-10-9.

Supplementary Material Available: Tables listing thermal parameters and the derived hydrogen positions for **16** and **17** (4 pages); tables of calculated and observed structure factors for **16** and **17** (13 pages). Ordering information is given on any current masthead page.

Contribution from the Departments of Chemistry, University of Minnesota, Minneapolis, Minnesota 55455, and University of New Orleans, New Orleans, Louisiana 70122

Structures and Properties of Dibridged (μ-Oxo)diiron(III) Complexes. Effects of the Fe–O–Fe Angle

Richard E. Norman,[†] Richard C. Holz,[†] Stéphane Ménage,[†] Charles J. O'Connor,[‡] Jian H. Zhang,[‡] and Lawrence Que, Jr.*[,†]

Received May 14, 1990

A series of (μ-oxo)diiron(III) complexes of tris(2-pyridylmethyl)amine (TPA), $[Fe_2(TPA)_2O(L)](ClO_4)_n$, were synthesized and characterized where L represents the bridging ligands carbonate, hydrogen maleate, diphenyl phosphate, diphenylphosphinate, maleate, and phthalate. Together with the linear dichloride complex, this series of compounds provides a unique opportunity to systematically study the effects of the Fe–O–Fe angle (125–180°) on the electronic spectral and magnetic properties of the (μ-oxo)diiron(III) core. $[Fe_2(TPA)_2O(CO_3)](ClO_4)_2$·$2CH_3OH$ (**1**) crystallizes in the monoclinic space group $P2_1/c$ with a = 11.282 (7) Å, b = 18.253 (9) Å, c = 20.390 (7) Å, and β = 95.02 (4)°. The structure was determined at −50 °C from 4544 out of a total of 8154 reflections with R = 0.068 and R_w = 0.080. $[Fe_2(TPA)_2O(maleateH)](ClO_4)_3$·$2CH_3COCH_3$ (**4**) crystallizes in the monoclinic space group $P2_1/n$ with a = 21.604 (6) Å, b = 11.76 (1) Å, c = 22.150 (7) Å, and β = 115.62 (3)°. The structure was determined at −50 °C from 4832 out of a total of 7043 reflections with R = 0.072 and R_w = 0.089. $[Fe_2(TPA)_2O(phthalate)](ClO_4)_2$·$CH_3OH$·$H_2O$ (**9**) crystallizes in the monoclinic space group $P\bar{1}$ with a = 12.170 (5) Å, b = 12.982 (9) Å, c = 17.070 (7) Å, α = 77.26 (7)°, β = 115.62 (3)°, and γ = 62.76 (6)°. The structure was determined at −32 °C from 3592 out of a total of 8329 reflections with R = 0.059 and R_w = 0.069. X-ray crystallographic studies of **1**, **4**, and **9** establish the presence of a doubly bridged diiron core in which complexes **1** and **4** contain distinct iron centers bridged by μ-1,3-carboxylates while **9** exhibits a symmetric diiron core bridged by a μ-1,6-phthalate. These studies also reveal that the (μ-oxo)diiron(III) core expands on going from **1** to **4** to **9** due to the increasing bites of the bridging ligands. The Fe–O–Fe bond angles of **1**, **4**, and **9** are 125.4, 131.0, and 143.4°, respectively, while the Fe···Fe distances are 3.196, 3.261, and 3.402 Å, respectively. ^1H NMR spectra indicate that the iron(III) centers of **1** and **4** remain distinct in solution while **9** retains its symmetric structure. While the magnetic properties of the complexes appear to be independent of the Fe–O–Fe angle, the visible absorption features of the complexes systematically blue shift as the Fe–O–Fe angle increases. The latter trend suggests that the visible bands are dominated by oxo-to-Fe(III) charge-transfer transitions.

Introduction

The (μ-oxo)diiron(III) unit has been the subject of considerable interest among inorganic chemists for several years.[1-3] This interest has further intensified[4] due to the discovery of a (μ-oxo)bis(μ-carboxylato)diiron(III) core in methemerythrin[5] and an analogous (μ-oxo)(μ-carboxylato)diiron(III) core in *Escherichia coli* ribonucleotide reductase.[6] The electronic spectra of methemerythrin[7,8] and ribonucleotide reductase[9] are rich with absorption features stretching from the UV region to the near-IR region. On the basis of a study of $[Fe_2O(HEDTA)_2]^{2-}$,[10] these features were initially proposed[11] to arise from simultaneous pair excitations of ligand field transitions, the forbiddenness of these transitions being partially lifted by the presence of antiferromagnetic coupling between the iron centers. However, more recent studies[7] on hemerythrin, employing a combination of polarized

(1) (a) Murray, K. S. *Coord. Chem. Rev.* **1974**, *12*, 1–35. (b) Kurtz, D. M., Jr. *Chem. Rev.* **1990**, *90*, 585–606.
(2) Ercolani, C.; Gardini, M.; Murray, K. S.; Pennesi, G.; Rossi, G. *Inorg. Chem.* **1986**, *25*, 3972–3976.
(3) Mukherjee, R. N.; Stack, T. D. P.; Holm, R. H. *J. Am. Chem. Soc.* **1988**, *110*, 1850–1861.
(4) (a) Que, L., Jr.; True, A. E. *Prog. Inorg. Chem.*, in press. (b) Sanders-Loehr, J. In *Iron Carriers and Iron Proteins*, Loehr, T. M., Ed.; VCH: New York, 1989; pp 373–466. (c) Que, L., Jr.; Scarrow, R. C. *ACS Symp. Ser.* **1988**, *372*, 152–178. (d) Lippard, S. J. *Angew. Chem., Intl. Ed. Engl.* **1988**, *27*, 344–361.
(5) (a) Stenkamp, R. E.; Sieker, L. C.; Jensen, L. H. *J. Am. Chem. Soc.* **1984**, *106*, 618–622. (b) Klotz, I. M.; Kurtz, D. M., Jr. *Acc. Chem. Res.* **1984**, *17*, 16–22.
(6) (a) Nordlund, P.; Sjöberg, B.-M.; Eklund, H. *Nature* **1990**, *345*, 593–598. (b) Reichard, P.; Ehrenberg, A. *Science (Washington, D.C.)* **1983**, *221*, 514–519. (c) Lynch, J. B.; Juarez-Garcia, C.; Münck, E.; Que, L., Jr. *J. Biol. Chem.* **1989**, *264*, 8091–8096.
(7) Reem, R. C.; McCormick, J. M.; Richardson, D. E.; Devlin, F. J.; Stephens, P. J.; Musselman, R. L.; Solomon, E. I. *J. Am. Chem. Soc.* **1989**, *111*, 4688–4704.
(8) Sanders-Loehr, J.; Loehr, T. M.; Mauk, A. G.; Gray, H. B. *J. Am. Chem. Soc.* **1980**, *102*, 6992–6996.
(9) Petersson, L.; Gräslund, A.; Ehrenberg, A.; Sjöberg, B.-M.; Reichard, P. *J. Biol. Chem.* **1980**, *255*, 6706–6712.
(10) The following abbreviations are used throughout: HEDTA, *N*-(hydroxyethyl)ethylenediamine-*N*,*N*′,*N*′-triacetic acid; HDP, *N*-(2-hydroxybenzyl)-*N*,*N*-bis(2-pyridylmethyl)amine; TPA, tris(2-pyridylmethyl)amine; Me_3tacn, 1,4,7-trimethyl-1,4,7-triazacyclononane; HB($pz)_3$, hydrotris(pyrazolyl)borate; BPA, bis(2-pyridylmethyl)amine; BBA, bis(2-benzimidazolylmethyl)amine; tpbn, *N*,*N*,*N*′,*N*′-tetrakis(2-pyridylmethyl)-1,4-diaminobutane.
(11) Schugar, H. J.; Rossman, G. R.; Barraclough, C. G.; Gray, H. B. *J. Am. Chem. Soc.* **1972**, *94*, 2683–2690.

0020-1669/90/1329-4629$02.50/0

Table I. Elemental Analyses of the Newly Synthesized TPA Complexes

complex	anal., % calcd C	H	N	Cl	found C	H	N	Cl
$[Fe_2(TPA)_2O(CO_3)](ClO_4)_2\cdot 2MeOH$ (**1**) $C_{39}H_{44}Cl_2Fe_2N_8O_{14}$	45.42	4.30	10.86		45.53	4.62	10.72	
$[Fe_2(TPA)_2O(maleateH)](ClO_4)_3\cdot 2$ acetone (**4**) $C_{46}H_{51}Cl_3Fe_2N_8O_{19}$	44.63	4.15	9.05	8.59	44.36	4.19	9.15	8.45
$[Fe_2(TPA)_2O(O_3P\{OPh\})](ClO_4)_2\cdot CH_3OH$ (**5**) $C_{43}H_{45}Cl_2Fe_2N_8O_{14}$	46.43	4.05	10.08		46.46	4.06	10.04	
$[Fe_2(TPA)_2O(O_2P\{Ph\}_2)](ClO_4)_3$ (**6**) $C_{48}H_{46}Cl_3Fe_2N_8O_{15}$	47.09	3.76	9.16		47.20	3.80	9.04	
$[Fe_2(TPA)_2O(phthalate)](ClO_4)_2\cdot MeOH\cdot H_2O$ (**9**) $C_{45}H_{46}Cl_2Fe_2N_8O_{15}$	48.19	4.13	9.99	6.32	48.29	4.10	9.99	6.31
$[Fe_2(TPA)_2OCl_2](ClO_4)_2$ (**10**) $C_{36}H_{36}Cl_4Fe_2N_8O_9$	44.22	3.69	11.47	14.54	44.20	3.92	11.46	14.52

Table II. Crystal Structure Parameters of $[Fe_2O(TPA)_2(L)](ClO_4)_n$ Complexes

	1, L = CO_3	**4**, L = malH	**9**, L = phthal
empirical formula	$C_{37}H_{36}Cl_2Fe_2N_8O_{12}$	$C_{40}H_{38}Cl_3Fe_2N_8O_{13}$	$C_{44}H_{40}Cl_2Fe_2N_8O_{13}$
fw	967.34	1056.85	1071.44
lattice params			
a, Å	11.282 (7)	21.604 (6)	12.170 (5)
b, Å	18.253 (9)	11.76 (1)	12.982 (9)
c, Å	20.390 (7)	22.150 (7)	17.070 (6)
α, deg	90	90	77.26 (7)
β, deg	95.02 (4)	115.62 (3)	70.67 (3)
γ, deg	90	90	62.76 (6)
V, Å^3	4183 (6)	5074 (6)	2255 (5)
space group	$P2_1/c$ (No. 14)	$P2_1/n$ (No. 14)	$P\bar{1}$ (No. 2)
Z	4	4	2
D_{calc}, g cm^{-3}	1.536	1.384	1.578
μ, cm^{-1}	8.89	7.38	8.34
radiation		Mo Kα (λ = 0.71069 Å)	
temp, °C	−50	−50	−32
residuals:[a] R, R_w	0.059, 0.069	0.068, 0.080	0.072, 0.089

[a] $R = \sum||F_o| - |F_c||/\sum|F_o|$; $R_w = [(\sum w(|F_o| - |F_c|)^2/\sum wF_o^2)]^{1/2}$.

UV–vis and CD techniques on single crystals and solutions, suggested that all of these features were explicable in terms of single-transition excited states. Thus the near-IR band observed near 1000 nm was assigned to the $^6A_1 \rightarrow {}^4T_1$ transition, the 600–750-nm band to the $^6A_1 \rightarrow {}^4T_2$ transition, the 400-550-nm features to a combination of the $^6A_1 \rightarrow ({}^4A, {}^4E)$ transitions and weak oxo-to-Fe(III) charge-transfer transitions, and the near-UV features principally to oxo-to-Fe(III) charge-transfer transitions.

We have recently reported the syntheses, structures, and spectral properties of (μ-oxo)diiron(III) complexes of tris(2-pyridylmethyl)amine (TPA) with a single carboxylate bridge, i.e. $[Fe_2(TPA)_2O(O_2X)](ClO_4)_3$,[12] where X is CH_3C and PhC. Complexes of this type share many of the physical properties of the related tribridged complexes and appear ideal to explore the effects of altering the Fe–O–Fe angle on the physical properties of the (μ-oxo)diiron(III) core. By replacement of the carboxylate bridge with ligands having larger "bite" angles, the Fe–O–Fe angle can be systematically altered. Reported herein are X-ray crystallographic data for the carbonate- (**1**), hydrogen maleate- (**4**), and phthalate- (**9**) bridged complexes. Together with the previously reported acetate (**2**), benzoate (**3**), and diphenyl phosphate (**7**) complexes and the linear dichloride complex,[13] these complexes afford a series wherein the Fe–O–Fe angle varies from 125 to 180°. The magnetic and electronic spectral properties of these structurally characterized complexes are compared; the properties of the related phenyl phosphate (**5**), diphenylphosphinate (**6**), and maleate (**8**) complexes are also included.

Experimental Methods

Synthetic Methods. $TPA\cdot 3HClO_4$ was synthesized according to literature procedures,[14,15] while all other chemicals were purchased commercially and used as received. *Caution! The perchlorate salts in this study are all potentially explosive and should be handled with care.*

The various $[Fe_2(TPA)_2O(L)](ClO_4)_x$[16] complexes were all synthesized in a similar manner. A typical preparation is as follows:[12b] $TPA\cdot 3HClO_4$ (0.59 g, 1.0 mmol) and triethylamine (0.56 mL, 4.0 mmol) in 40 mL of MeOH were reacted with $Fe(ClO_4)_3\cdot 10H_2O$ (0.54 g, 1.0 mmol) dissolved in 2 mL of MeOH. To this mixture was added a solution of the bridging ligand (0.5 mmol) and triethylamine (0.5 or 1.0 mmol, depending on the number of protons to be neutralized) in MeOH (≈2 mL). When this mixture was allowed to stand, microcrystals of the desired complex were obtained. Table I lists the elemental analyses of the newly synthesized complexes.

$[Fe_2(TPA)_2OCl_2](ClO_4)_2$ (**10**) was prepared as follows: $TPA\cdot 3HClO_4$ (0.59 g, 1.0 mmol) and triethylamine (0.56 mL, 4.0 mmol) in 40 mL of MeOH were reacted with $FeCl_3\cdot 6H_2O$ (0.27 g, 1.0 mmol) dissolved in 2 mL of MeOH. A turbid yellow solution resulted, which became dark brown and nonturbid upon the addition of excess base. The complex was crystallized by vapor diffusion of diethyl ether into the resulting filtered methanol solution.

Crystallographic Studies. Crystals of **1** and **4** suitable for X-ray diffraction studies were grown from acetone solutions placed in an ethyl acetate bath. Crystals of **9** suitable for X-ray studies were obtained directly from the reaction mixture. The crystals were mounted on glass

(12) (a) Yan, S.; Cox, D. D.; Pearce, L. L.; Juarez-Garcia, C.; Que, L., Jr.; Zhang, J. H.; O'Connor, C. J. *Inorg. Chem.* **1989**, *28*, 2507–2509. (b) Norman, R. E.; Yan, S.; Que, L., Jr.; Backes, G.; Ling, J.; Sanders-Loehr, J.; Zhang, J. H.; O'Connor, C. J. *J. Am. Chem. Soc.* **1990**, *112*, 1554–1562.

(13) The structural information on the linear $[Fe_2O(TPA)_2Cl_2]^{2+}$ ion is derived from a crystallographic study of $[Fe(TPA)Cl_2]_2[Fe_2O(TPA)_2Cl_2](ClO_4)_4$. Crystal data at 183 K: monoclinic space group $P2_1/c$ (No. 14), a = 13.772 (9) Å, b = 12.671 (6) Å, c = 23.621 (11) Å, β = 91.53 (4)°, V = 4121 (7) Å^3, Z = 2. For 3660 unique reflections with $I > 1.0\sigma(I)$ and 449 variable parameters, the current discrepancy indices are R = 0.065 and R_w = 0.055. Complete details will be published in a subsequent manuscript.

(14) Anderegg, G.; Wenk, F. *Helv. Chim. Acta* **1967**, *50*, 2330–2332.

(15) Gafford, B. G.; Holwerda, R. A. *Inorg. Chem.* **1989**, *28*, 60–66.

(16) Although these complexes can be crystallized in various solvated forms (i.e. complex·2H_2O, complex·2 acetone, etc.), the solvent molecules are lost upon dissolution. To avoid confusion, we ignore the state of solvation when referring to the complexes throughout the text.

Table III. Positional and Thermal Parameters for Selected Atoms of $[Fe_2(TPA)_2O(L)](ClO_4)_n$ Complexes

atom	x	y	z	B_{eq}, Å^2
		L = CO_3 (**1**)		
Fe1	0.49159 (9)	0.20208 (7)	0.65886 (6)	2.05 (4)
Fe2	0.7461 (1)	0.20431 (8)	0.74159 (6)	2.65 (5)
O12	0.6486 (4)	0.1790 (3)	0.6717 (3)	2.1 (2)
C1	0.5297 (7)	0.2770 (4)	0.7876 (4)	2.6 (3)
O2	0.6364 (5)	0.2512 (5)	0.7975 (3)	4.5 (3)
O3	0.4730 (5)	0.2691 (3)	0.7292 (3)	3.0 (3)
O4	0.4829 (5)	0.3089 (3)	0.8316 (3)	3.2 (3)
N1A	0.4577 (6)	0.1296 (4)	0.5728 (3)	2.4 (3)
N2A	0.4424 (5)	0.1008 (4)	0.7016 (3)	2.5 (3)
N3A	0.3010 (5)	0.2198 (3)	0.6296 (4)	2.5 (3)
N4A	0.5131 (5)	0.2735 (4)	0.5793 (3)	2.4 (3)
N1B	0.8878 (6)	0.2329 (5)	0.8217 (4)	3.8 (4)
N2B	0.8132 (5)	0.3078 (4)	0.7107 (4)	2.9 (3)
N3B	0.9023 (6)	0.1542 (4)	0.7073 (4)	2.7 (3)
N4B	0.7550 (7)	0.1098 (6)	0.8055 (4)	4.3 (4)
		L = malH (**4**)		
Fe1	0.50683 (6)	0.4420 (1)	0.29538 (6)	1.78 (4)
Fe2	0.58500 (6)	0.2022 (1)	0.30059 (6)	1.60 (4)
O1	0.5134 (3)	0.2959 (5)	0.2735 (3)	1.8 (2)
O1C	0.6600 (3)	0.3110 (5)	0.3595 (3)	1.8 (2)
O2C	0.6034 (3)	0.4688 (5)	0.3590 (3)	2.5 (2)
C1C	0.6570 (4)	0.4125 (8)	0.3743 (4)	2.0 (3)
C2C	0.7223 (4)	0.4735 (8)	0.4166 (4)	2.5 (3)
C3C	0.7746 (4)	0.4828 (8)	0.3995 (5)	2.8 (4)
C4C	0.7704 (5)	0.4410 (9)	0.3341 (6)	3.3 (4)
O3C	0.8265 (4)	0.396 (1)	0.3360 (6)	9.3 (6)
O4C	0.7198 (4)	0.4439 (6)	0.2821 (3)	3.6 (3)
N1A	0.3989 (3)	0.4726 (6)	0.2282 (4)	2.4 (3)
N2A	0.4550 (3)	0.4054 (6)	0.3562 (4)	2.1 (3)
N3A	0.4937 (3)	0.6208 (6)	0.3182 (4)	2.3 (3)
N4A	0.5108 (4)	0.5113 (6)	0.2077 (3)	2.2 (3)
N1B	0.6719 (3)	0.0779 (6)	0.3333 (4)	2.3 (3)
N2B	0.6251 (3)	0.2227 (6)	0.2285 (3)	2.2 (3)
N3B	0.5336 (3)	0.0563 (6)	0.2478 (3)	2.1 (3)
N4B	0.5881 (3)	0.1287 (6)	0.3899 (3)	1.9 (3)
		L = phthal (**9**)		
Fe1	0.20815 (8)	0.26927 (9)	0.76810 (5)	1.57 (8)
Fe2	0.51166 (8)	0.2448 (1)	0.67239 (6)	1.72 (8)
O12	0.3766 (4)	0.2298 (4)	0.7481 (3)	2.1 (4)
O1C	0.1693 (4)	0.3649 (4)	0.6688 (3)	2.2 (4)
O2C	0.4366 (4)	0.3281 (5)	0.5794 (3)	2.4 (4)
O3C	0.0820 (7)	0.5580 (6)	0.6694 (4)	5.6 (7)
O4C	0.4315 (6)	0.1980 (5)	0.5171 (4)	4.4 (6)
C1C	0.1818 (6)	0.4773 (7)	0.5392 (4)	2.0 (6)
C2C	0.2947 (6)	0.3932 (6)	0.4947 (4)	2.0 (6)
C3C	0.3203 (7)	0.4009 (7)	0.4077 (4)	2.6 (7)
C4C	0.1246 (7)	0.5713 (7)	0.4112 (4)	2.9 (7)
C5C	0.2359 (8)	0.4875 (8)	0.3670 (4)	3.3 (8)
C6C	0.0985 (7)	0.5649 (7)	0.4971 (4)	2.6 (7)
C7C	0.1418 (7)	0.4700 (7)	0.6334 (4)	2.5 (7)
C8C	0.3936 (6)	0.2977 (7)	0.5339 (4)	2.5 (7)
N1A	0.2132 (5)	0.1407 (5)	0.8766 (3)	1.9 (5)
N2A	0.1708 (5)	0.3693 (5)	0.8652 (3)	2.1 (5)
N3A	0.0040 (5)	0.3049 (5)	0.8251 (3)	1.9 (5)
N4A	0.2409 (5)	0.1157 (5)	0.7203 (3)	2.2 (5)
N1B	0.6333 (5)	0.1945 (6)	0.7593 (3)	2.1 (5)
N2B	0.6133 (5)	0.0555 (5)	0.6696 (3)	1.9 (5)
N3B	0.7028 (5)	0.2306 (5)	0.5880 (3)	2.3 (5)
N4B	0.4687 (5)	0.4072 (5)	0.7156 (3)	2.1 (5)

fibers and coated with a viscous hydrocarbon. All data were collected on an Enraf-Nonius CAD4 diffractometer using graphite-monochromated Mo Kα (λ = 0.71069 Å) radiation and the ω-scan method. All data were corrected for Lorentz and polarization effects. Some pertinent crystallographic details for **1**, **4**, and **9** are collected in Table II while the fractional atomic coordinates and thermal factors of significant atoms are listed in Table III. Further details including the complete listing of the fractional atomic coordinates, thermal factors, and bond lengths and angles are provided in the supplementary material. Some specific details of each structure are discussed below. Each structure was solved by using direct methods.[17] Hydrogen atoms were placed in calculated positions, assigned thermal parameters that were 20% greater than the B_{eq} value of the atom to which they were bonded, and not refined. All ordered non-hydrogen atoms were refined anisotropically. Refinement was carried out by using full-matrix least-squares methods on F, with scattering factors from ref 18 and included anomalous dispersion terms.[19]

Three standard reflections were measured every 100 min for **1**, **4**, and **9** and in each case showed negligible decay. Each data set was also corrected for absorption. The structure solution and refinement proceeded normally for **1** with the exception of disordered solvent molecules, which have been modeled with three carbon atoms. While the perchlorate anions are likely to be disordered,[20] the structure refined acceptably with further treatment of the disorder.

The structure solution and refinement proceeded normally for **4** with the exceptions of the perchlorate anions (which were disordered and were modeled with rigid groups in three positions of 0.57, 0.30, and 0.13 occupancy for $ClO_4(1)$; 0.58, 0.30, and 0.12 occupancy for $ClO_4(2)$; and 0.41, 0.36, and 0.23 occupancy for $ClO_4(3)$) and a disordered solvent molecule (modeled with two carbon atoms) near the noncoordinated carboxylate group.

The structure solution and refinement for **9** proceeded normally with the exception of the perchlorate anions (which were disordered and were modeled with rigid groups in two positions of 0.57 and 0.43 occupancy for $ClO_4(1)$ and 0.56 and 0.44 occupancy for $ClO_4(2)$).

Physical Methods. Visible spectra were recorded on a Hewlett-Packard 8541A diode array spectrometer. ^{1}H NMR spectra were recorded on an IBM AC 300 spectrometer at 300 MHz. Chemical shifts (in ppm) were referenced to residual protic solvent peaks. Magnetic susceptibility data were recorded over a temperature range of 10–300 K at a measuring field of 2.0 kOe with an SHE Corp. VTS-50 superconducting SQUID susceptometer interfaced to an IBM 9000 computer system. Calibration and operating procedures have been reported elsewhere.[21]

Results and Discussion

The explosion of synthetic studies related to the (μ-oxo)diiron(III) site in proteins has contributed greatly to our understanding of the fundamental properties of this structural motif.[4,22,23] However, no systematic series of compounds to date has allowed us to assess the effects of the Fe–O–Fe angle on the electronic spectral and magnetic properties of complexes with (μ-oxo)diiron(III) cores. With $[Fe_2(TPA)_2O(L)](ClO_4)_x$ complexes, we have obtained such a series of compounds where the Fe–O–Fe angle has been varied by changing the "bite" angle of the supporting bridge. The crystal structures of the complexes where L is carbonate (**1**), hydrogen maleate (**4**), or phthalate (**9**) are discussed below; structures for the complexes where L is acetate (**2**), benzoate (**3**), and diphenyl phosphate (**7**) have been reported previously.[12b] Also included in this study are derivatives where L is phenyl phosphate (**5**) or diphenylphosphinate (**6**); though not crystallographically characterized, they are expected to have bites similar to that of diphenyl phosphate, on the basis of information

(17) Gilmore, C. J. *J. Appl. Crystallogr.* **1984**, *17*, 42–46.

(18) Cromer, D. T.; Waber, J. T. *International Tables for X-ray Crystallography*; Kynoch Press: Birmingham, England, 1974; Vol. IV, Table 2.2 A.

(19) Cromer, D. T. *International Tables for X-ray Crystallography*; Kynoch Press: Birmingham, England, 1974; Vol. IV, Table 2.3.1.

(20) The highest residual electron density (1.0 electron/Å^3) is associated with the perchlorates.

(21) O'Connor, C. J. *Prog. Inorg. Chem.* **1979**, *29*, 204–283.

(22) (a) Chaudhuri, P.; Wieghardt, K.; Nuber, B.; Weiss, J. *Angew. Chem., Int. Ed. Engl.* **1985**, *24*, 778–779. (b) Hartman, J. R.; Rardin, R. L.; Chaudhuri, P.; Pohl, K.; Wieghardt, K.; Nuber, B.; Weiss, J.; Papaefthymiou, G. C.; Frankel, R. B.; Lippard, S. J. *J. Am. Chem. Soc.* **1987**, *109*, 7387–7396. (c) Armstrong, W. H.; Spool, A.; Papaefthymiou, G. C.; Frankel, R. B.; Lippard, S. J. *J. Am. Chem. Soc.* **1984**, *106*, 3653–3667. (d) Toftlund, H.; Murray, K. S.; Zwack, P. R.; Taylor, L. F.; Anderson, O. P. *J. Chem. Soc., Chem. Commun.* **1986**, 191–193. (e) Gomez-Romero, P.; Casan-Pastor, N.; Ben-Hussein, A.; Jameson, G. B. *J. Am. Chem. Soc.* **1988**, *110*, 1988–1990. (f) Vincent, J. B.; Huffman, J. C.; Christou, G.; Li, Q.; Nanny, M. A.; Hendrickson, D. N.; Fong, R. H.; Fish, R. H. *J. Am. Chem. Soc.* **1988**, *110*, 6898–6900. (g) Feng, X.; Bott, S. G.; Lippard, S. J. *J. Am. Chem. Soc.* **1989**, *111*, 8046–8047.

(23) (a) Armstrong, W. H.; Lippard, S. J. *J. Am. Chem. Soc.* **1985**, *107*, 3730–3731. (b) Turowski, P. N.; Armstrong, W. H.; Roth, M. E.; Lippard, S. J. *J. Am. Chem. Soc.* **1990**, *112*, 681–690. (c) Drücke, S.; Wieghardt, K.; Nuber, B.; Weiss, J.; Fleischhauer, H.-P.; Gehring, S.; Haase, W. *J. Am. Chem. Soc.* **1989**, *111*, 8622–8631.

Table IV. Relevant Distances and Angles for $[Fe_2O(TPA)_2(L)](ClO_4)_n$ Complexes

param[a]	1, L = CO_3	4, L = malH	9, L = phthal
Fe1···Fe2	3.196 (2)	3.261 (2)	3.402 (2)
Fe1–O12	1.817 (5)	1.808 (6)	1.799 (5)
Fe2–O12	1.784 (5)	1.779 (5)	1.785 (5)
Fe1–O3	1.911 (6)	1.973 (5)	1.924 (5)
Fe2–O2	1.953 (6)	2.034 (5)	1.956 (5)
Fe1–N1A	2.204 (7)	2.187 (6)	2.200 (6)
Fe1–N2A	2.137 (7)	2.140 (3)	2.133 (7)
Fe1–N3A	2.205 (6)	2.209 (8)	2.209 (6)
Fe1–N4A	2.112 (7)	2.143 (8)	2.139 (7)
Fe2–N1B	2.245 (7)	2.239 (7)	2.228 (7)
Fe2–N2B	2.149 (8)	2.133 (9)	2.192 (6)
Fe2–N3B	2.156 (8)	2.103 (7)	2.242 (6)
Fe2–N4B	2.158 (9)	2.133 (8)	2.164 (8)
Fe1–O12–Fe2	125.4 (3)	131.0 (3)	143.4 (3)
O12–Fe–N1A	94.2 (2)	99.1 (2)	90.9 (2)
O12–Fe1–N2A	91.5 (2)	95.8 (3)	89.2 (3)
O12–Fe1–N3A	171.2 (3)	177.2 (2)	165.7 (2)
O12–Fe1–N4A	94.4 (2)	94.6 (3)	93.0 (3)
O12–Fe1–O3	102.1 (2)	99.4 (2)	102.5 (2)
N1A–Fe1–N2A	76.8 (3)	76.5 (3)	78.5 (2)
N1A–Fe1–N3A	77.0 (3)	78.2 (3)	76.7 (2)
N1A–Fe1–N4A	77.5 (3)	76.7 (3)	75.3 (2)
N1A–Fe1–O3	163.6 (2)	161.2 (3)	162.5 (3)
N2A–Fe1–N3A	87.4 (2)	83.9 (3)	81.3 (3)
N2A–Fe1–N4A	154.0 (3)	152.5 (3)	153.7 (2)
N2A–Fe1–O3	101.4 (3)	105.2 (3)	112.3 (2)
N3A–Fe1–N4A	82.9 (2)	84.5 (3)	90.8 (3)
N3A–Fe1–O3	86.6 (2)	83.4 (2)	91.0 (2)
N4A–Fe1–O3	102.1 (3)	98.2 (3)	92.7 (2)
O12–Fe2–N1B	172.7 (3)	177.5 (2)	96.5 (2)
O12–Fe2–N2B	101.6 (3)	104.6 (3)	90.3 (2)
O12–Fe2–N3B	95.5 (3)	98.3 (3)	169.1 (2)
O12–Fe2–N4B	105.6 (3)	103.7 (3)	92.9 (3)
O12–Fe2–O2	101.7 (3)	99.4 (2)	100.6 (2)
N1B–Fe2–N2B	76.2 (3)	76.2 (3)	76.8 (3)
N1B–Fe2–N3B	77.6 (3)	79.3 (3)	76.2 (2)
N1B–Fe2–N4B	75.8 (3)	75.5 (3)	75.4 (3)
N1B–Fe2–O2	85.4 (3)	83.0 (2)	158.5 (3)
N2B–Fe2–N3B	87.7 (3)	88.0 (3)	80.2 (2)
N2B–Fe2–N4B	151.6 (3)	151.6 (3)	152.1 (3)
N2B–Fe2–O2	92.5 (3)	86.6 (3)	115.7 (3)
N3B–Fe2–N4B	82.0 (3)	88.9 (3)	93.1 (3)
N3B–Fe2–O2	162.5 (3)	162.3 (3)	88.3 (2)
N4B–Fe2–O2	105.6 (3)	87.9 (2)	90.9 (3)

[a] All distances are in Å, and all angles are in deg. For labels, see the ORTEP drawings. O2 and O3 are the carboxylate labels.

on related structures.[23] Similarly, the maleate derivative (**8**) is expected to be structurally similar to the phthalate complex (**9**). To cap the series, we also include the dichloride complex (**10**),

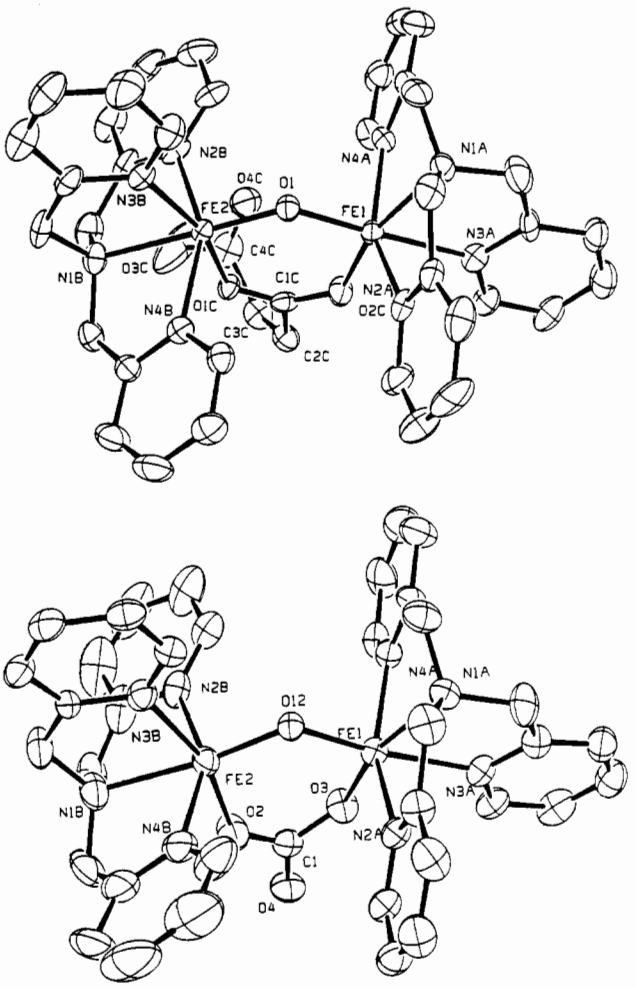

Figure 1. ORTEP drawings of (a, top) $[Fe_2(TPA)_2O(maleateH)]^{3+}$ and (b, bottom) $[Fe_2(TPA)_2O(CO_3)]^{2+}$ showing a partial numbering scheme (carbon atoms are not labelled; a diagram of the ligand atom numbering scheme is included in the supplementary material). The hydrogen atoms are omitted for clarity, and each complex is numbered similarly. The TPA ligand with "A" labels is bound to Fe1 and has N3A (a pyridine nitrogen) trans to the μ-oxo bridge, while the TPA ligand with "B" labels is bound to Fe2 and has N1B (a tertiary amine nitrogen) trans to the μ-oxo bridge.

which has a linear Fe–O–Fe unit.[13]

Crystallographic Studies. X-ray diffraction studies have been conducted on complexes **1**, **4**, and **9**. Relevant distances and angles of these complexes are collected in Table IV and pertinent parameters are compared with those of related complexes in Table V. The structures of **1** and **4** are quite similar to those of **2** and

Table V. Comparison of Relevant Distances and Angles for $[Fe_2O(TPA)_2(L)](ClO_4)_n$ Complexes[a]

feature[b]	1	2	3	4	7	9
Fe···Fe	3.196 (2)	3.243 (1)	3.241 (1)	3.261 (2)	3.357 (3)	3.402 (2)
	125.4 (3)	129.2 (2)	129.7 (3)	131.0 (3)	138.1 (2)	143.4 (3)
Fe–O_b	1.817 (5)[e]	1.799 (4)[e]	1.808 (3)[e]	1.808 (6)[e]	1.815 (5)[e]	1.799 (5)[e]
	1.784 (5)[f]	1.790 (3)[f]	1.774 (3)[f]	1.779 (5)[f]	1.779 (3)[f]	1.785 (5)[f]
Fe–N(tertiary)	2.204 (7)[e]	2.198 (3)[e]	2.190 (4)[e]	2.187 (6)[e]	2.178 (4)[e]	2.200 (6)[e]
	2.245 (7)[c,f]	2.237 (4)[c,f]	2.221 (4)[c,f]	2.239 (7)[c,f]	2.239 (4)[c,f]	2.228 (7)[f]
Fe–O_{acido}	1.911 (6)[d,e]	1.974 (3)[d,e]	1.980 (3)[d,e]	1.973 (5)[d,e]	1.963 (3)[d,e]	1.924 (5)[d,e]
	1.953 (6)[f]	2.036 (4)[f]	2.045 (3)[f]	2.034 (5)[f]	2.045 (3)[f]	1.956 (5)[d,f]
Fe–N_{ar}	2.112 (7)[e]	2.126 (4)[e]	2.131 (4)[e]	2.140 (1)[e]	2.122 (4)[e]	2.133 (7)[e]
	2.137 (7)[e]	2.124 (6)[e]	2.114 (4)[e]	2.143 (8)[e]	2.130 (4)[e]	2.139 (7)[e]
	2.205 (6)[c,e]	2.200 (6)[c,e]	2.182 (4)[c,e]	2.209 (8)[c,e]	2.184 (4)[c,e]	2.209 (6)[c,e]
	2.149 (8)[f]	2.133 (4)[f]	2.130 (4)[f]	2.133 (8)[f]	2.121 (4)[f]	2.192 (6)[f]
	2.156 (8)[f]	2.157 (4)[f]	2.140 (4)[f]	2.133 (9)[f]	2.127 (4)[f]	2.164 (8)[f]
	2.158 (9)[f]	2.105 (4)[f]	2.122 (4)[f]	2.103 (7)[f]	2.130 (4)[f]	2.242 (6)[c,f]

[a] All distances are in Å, and all angles are in deg. Complexes with bridging carbonate (**1**), acetate (**2**), benzoate (**3**), hydrogen maleate (**4**), diphenyl phosphate (**7**), and phthalate (**9**). [b] O_b refers to the oxo bridge. N(tertiary) refers to the tertiary amine nitrogen. O_{acido} refers to the oxygen atoms of carboxylate or phosphate bridges. N_{ar} refers to aromatic nitrogen atoms. [c] These atoms are trans to the oxo bridge. [d] This oxygen atom is trans to the tertiary amine. [e] Distances corresponding to Fe1. [f] Distances corresponding to Fe2.

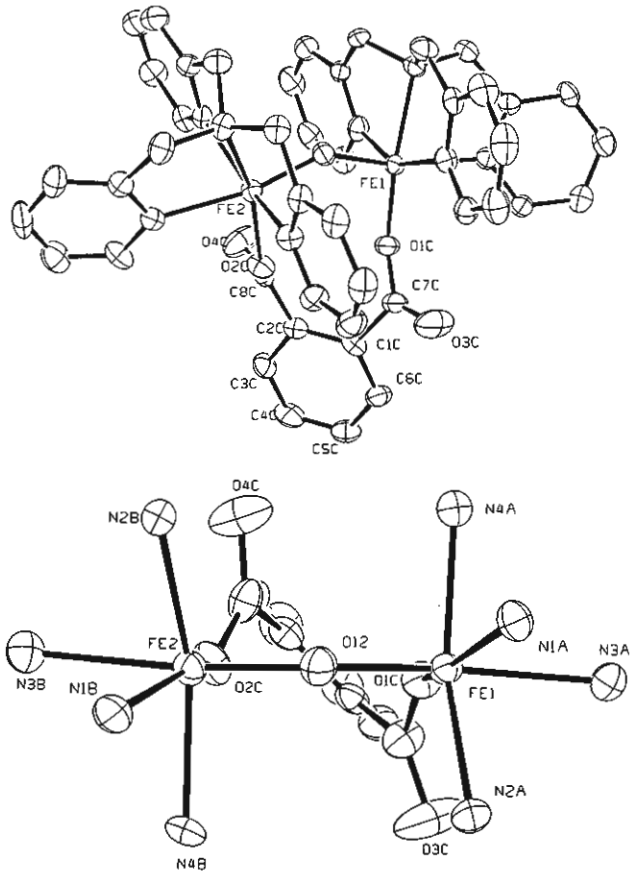

Figure 2. ORTEP drawings of $[Fe_2(TPA)_2O(phthalate)]^{2+}$: (a, top) view with hydrogen atoms omitted for clarity; (b, bottom) view looking down the effective 2-fold axis, with the nonligating TPA atoms omitted. The molecule has an effective 2-fold axis relating the two iron sites, which is emphasized in view b.

3 in that the (μ-oxo)(μ-carboxylato)diiron(III) cores contain distinct iron sites (Figure 1).[12b] On Fe1 the tertiary amine is cis to the oxo bridge, while the tertiary amine on Fe2 is trans to the oxo bridge. This difference of ligand configuration produces the expected differences[12b] in the Fe–ligand bond lengths found in the Fe–O_b, Fe–N1, Fe–N3, and Fe–O_{COO} bonds. The core dimensions of **4** compare well with those of the acetate and benzoate complexes, although the Fe···Fe separation is somewhat larger. The other carboxylate group of the maleate ligand retains its proton and is thus not coordinated; this proton is hydrogen bonded to one of the perchlorate anions in the crystal lattice.

The core dimensions of **1** differ somewhat from those of the acetate and benzoate complexes, presumably due to the nature of the carbonate bridge. The higher charge and basicity of the carbonate result in a stronger Fe–carbonate interaction as indicated by shorter Fe–O bonds (an average of 1.93 Å for **1** vs 2.01 Å for **2**–**4**) and a slight weakening of the bonds to the oxo bridge (average of 1.80 Å for **1** vs 1.79 Å for **2**–**4**) and the TPA ligands (average Fe–N bond of 2.17 Å for **1** vs 2.16 Å for **4**). All of these subtle changes contribute to a shorter Fe···Fe separation of 3.196 Å and a smaller Fe–O_b–Fe angle of 125.4°. As expected, the largest differences in the Fe–N distances are those trans to the carbonate, reflecting the larger trans effect of carbonate relative to carboxylate (Fe1–N1A is 2.204 Å and Fe2–N3B is 2.156 Å in **1** compared to 2.187 and 2.103 Å, respectively, for **4**). These effects (longer Fe–O_b distances, shorter Fe···Fe distances, a smaller Fe–O_b–Fe angle, and longer Fe–N distances trans to the carbonate) were also observed[24] in $[Fe_2(Me_3tacn)_2O(CO_3)_2]$ relative to $[Fe_2(Me_3tacn)_2O(OAc)_2]^{2+}$ and were similarly attributed to the tighter binding of carbonate relative to acetate.

(24) Drüeke, S.; Wieghardt, K.; Nuber, B.; Weiss, J. *Inorg. Chem.* **1989**, *28*, 1414–1417.

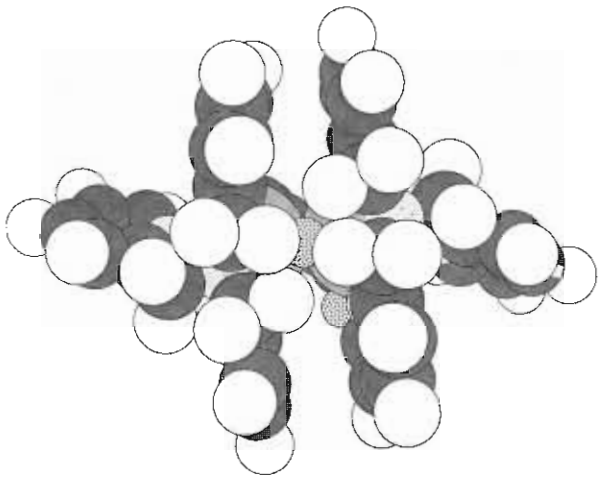

Figure 3. View of $[Fe_2(TPA)_2O(phthalate)]^{2+}$ emphasizing the ring stacking interactions.

The phthalate complex **9** retains the (μ-oxo)diiron(III) unit but exhibits a different structure (Figure 2). The phthalate ligand uses both carboxylate groups to bridge the diiron(III) unit with each carboxylate coordinated in a monodentate fashion to its respective iron center. This bridging arrangement effectively increases the "bite" of the bridging ligand and produces the expected increases in the Fe···Fe distance (3.402 Å) and the Fe–O_b–Fe angle (143.4°). This complex has effective 2-fold symmetry about the Fe–O–Fe unit bisecting the phthalate ring. The TPA ligands are coordinated to each iron atom with the tertiary amine nitrogens cis to the oxo bridge (Figure 2b).

The coordination mode of phthalate is of interest. Phthalate has been found to exhibit a variety of coordination modes, monodentate,[25] 1,3-chelating,[26] and 1,6-chelating,[27] and various bridging modes[28] including the 1,6-bridge found in *catena*-aqua(1,10-phenanthroline)(μ-phthalato)copper(II) hemihydrate[29] and in *catena*-(μ-phthalato)bis(oxamide oxime)nickel(II) tetrahydrate.[30] To our knowledge, **9** contains the first example of a 1,6-bridging phthalate in a discrete complex.

The phthalate complex is one of a few examples of structurally characterized iron carboxylate complexes where the carboxylate oxygen can choose which lone pair will be used in binding.[31] Most of the structurally characterized iron(III) carboxylate complexes involve either multidentate ligands in which the carboxylate must coordinate to the metal via the anti lone pair in order to complete the chelate ring or bridging carboxylates where the carboxylate must coordinate to the metal via the syn lone pair. A consideration of the stereoelectronic properties of the carboxylate oxygen lone pairs suggests that the syn lone pair is more basic and should thus be preferred for binding.[32] This preference is demonstrated in the phthalate complex (Figure 2b).

The observed TPA configurations of **1**, **4**, and **9** differ from those of the related HDP ligand, which affords a dibridged

(25) See, for example: Kozlova, N. P.; Agre, V. M.; Trunov, V. K.; Makarevich, S. S.; Barkhanova, N. N. *Russ. J. Struct. Chem.* (*Engl. Transl.*) **1982**, *23*, 746–751; *Zh. Struckt. Khim.* **1982**, *23*, 108–113.
(26) See, for example: Biagini Cingi, M.; Guastini, C.; Musatti, A.; Nardelli, M. *Acta Crystallogr.* **1969**, *B25*, 1833–1840.
(27) See, for example: Bats, J. W.; Kallel, A.; Fuess, H. *Acta Crystallogr.* **1978**, *B34*, 1705–1707.
(28) See, for example: Biagini Cingi, M.; Manotti Lanfredi, A. M.; Tiripicchio, A.; Tiripicchio Camellini, M. *Acta Crystallogr.* **1981**, *B37*, 2159–2163.
(29) Krstanovic, I.; Karanovic, Lj.; Stojakovic, Dj. *Acta Crystallogr.* **1985**, *C41*, 43–45.
(30) Endres, H. *Z. Anorg. Allg. Chem.* **1984**, *513*, 78–88.
(31) (a) Eremenko, I. L.; Pasynskii, A. A.; Orazsakhatov, B.; Ellert, O. G.; Novotortsev, V. M.; Kalinnikov, V. T.; Porai-Koshits, M. A.; Antsyshkina, A. S.; Dikareva, L. M.; Ostrikova, V. N.; Struchkov, Yu. T.; Gerr, R. G. *Inorg. Chim. Acta* **1983**, *73*, 225–229. (b) Oumous, H.; Lecomte, C.; Protas, J.; Cocolios, P.; Guilard, R. *Polyhedron* **1984**, *3*, 651–659.
(32) Carrell, C. J.; Carrell, H. L.; Erlebacher, J.; Glusker, J. P. *J. Am. Chem. Soc.* **1988**, *110*, 8651–8656 and references therein.

Table VI. ^{1}H NMR Parameters (ppm) of TPA Complexes

assignt	**1**, L = CO_3	**2**, L = OAc	**3**, L = OBz	**4**, L = malH	**5**, L = $O_3P(OPh)$	**6**, L = $O_2P(Ph)_2$	**7**, L = $O_2P(OPh)_2$	**8**, L = mal	**9**, L = phthal	**10**, L = Cl_2
py 2,6-H		36	37	37		40	42			
or CH_2	30	31	32	32	32	32	34	32	32	33
	27	23	23	23	29	25	26			29
	23	20	20	21	25	21	22	19	19	20
py 3,5-H	17.7	17.4	17.4	17.5	18.3	18.2	18.8	17.3	17.2	17.7
	16.7	16.4	16.6	16.6	17.4	17.4	17.9	16.3	16.2	16.7
	15.4				16.3					
	12.9	12.6	12.7	12.5	13.7	13.8	13.9	13.3	13.3	12.9
	12.2	12.3	12.3	11.3	13.2	13.0	13.2	12.0	12.1	11.5
	11.4	11.2	11.0		12.0	12.1	12.4			
py 4-H	7.5	7.9	8.0	8.0	7.8	8.5	8.0	7.7	8.1	7.5
	7.1	6.9	6.9	6.9	7.0	8.0	6.9	7.0	6.9	7.1
	6.6	6.5	6.5	6.4	6.9	6.9	6.5			
		6.4				6.6	6.2			
XO_2		14.0 (OAc)	9.2 (m-OBz)	15.5 (α-mal)				14.7 (mal)	8.8 (phthal)	
			6.7 (p-OBz)	9.5 (β-mal)					8.0 (sh) (phthal)	

complex $[Fe_2(HDP)_2O(OBz)]BPh_4$ with the tertiary amines trans to the oxo bridge.[33] Aliphatic amine nitrogens are also trans to the oxo bridge in (μ-oxo)bis(μ-carboxylato)diiron(III) complexes such as $[Fe_2(BBA)_2O(OAc)_2]^{2+}$ and $[Fe_2(tpbn)O(OAc)_2]_2^{4+}$, which have combinations of aliphatic and aromatic amines on the terminal faces.[22] The TPA ligands in **1** and **4** have the same configuration as in **2** and **3**. We have suggested previously[12b] that the symmetric configuration analogous to that found for the HDP complex is disfavored because of steric interactions engendered when pyridine replaces the phenolate of each ligand. These substitutions generated unfavorable steric contact between the C3H protons of pyridines coordinates to the two ferric ions. The unsymmetric TPA configuration adopted is thus a compromise between the electronic preference for a weaker ligand trans to the oxo bridge and steric constraints. Yet another factor appears to come into play when the Fe–O–Fe angle increases as observed in **9**. This complex exhibits a symmetric structure with the tertiary amines cis to the oxo bridge. An examination of the structure suggests that the ring-stacking interactions between the TPA pyridine rings become sufficiently favorable in **9** to overcome the preference of the oxo bridge to be trans to the amine nitrogens (Figure 3). This symmetric orientation of TPA (with the tertiary amines cis to an oxo bridge) is also observed for $[Cr_2(TPA)_2O(NCS)_2]^{2+}$,[34] which has a linear M–O–M unit. In all of the $[Fe_2(TPA)_2O(O_2X)]^{n+}$ complexes studied to date, it appears that there is a subtle interplay between steric constraints and bonding considerations that ultimately lead to the given structure, making it difficult to predict a priori which factors will dominate and what the resulting structure will be. Fortunately, it appears possible to determine the symmetry of the structures from NMR spectroscopy (vide infra).

^{1}H NMR. The ^{1}H NMR spectra of **4** and **9** are shown in parts a and c of Figure 4, respectively, and their chemical shifts are compared with those of several other complexes in Table VI. In both cases, the spectra confirm that the solid-state structure is retained in solution. For **4**, the ^{1}H NMR spectrum shows the pattern typical of unsymmetric TPA coordination,[12b] namely three peaks from 6.0 to 8.0 ppm (the region corresponding to the TPA pyridine 4-protons) of relative intensity 2:1:3, four broad features from 20 to 40 ppm (which may arise from either the CH_2 or pyridine 2,6-protons), and a complex splitting pattern from 10 to 20 ppm (the region corresponding to the TPA pyridine 3,5-protons). Similar spectral features are noted for **1**. The maleate protons are assigned on the basis of comparisons with the spectra of the acetate and benzoate derivatives. One feature, absent from the ^{1}H NMR spectra of **2** and **3** is noted at 9.5 ppm (relative intensity 1), which is assigned to the more distant maleate C3H proton. The peak arising from the maleate C2H proton is likely to be the broader feature at 15.5 ppm.

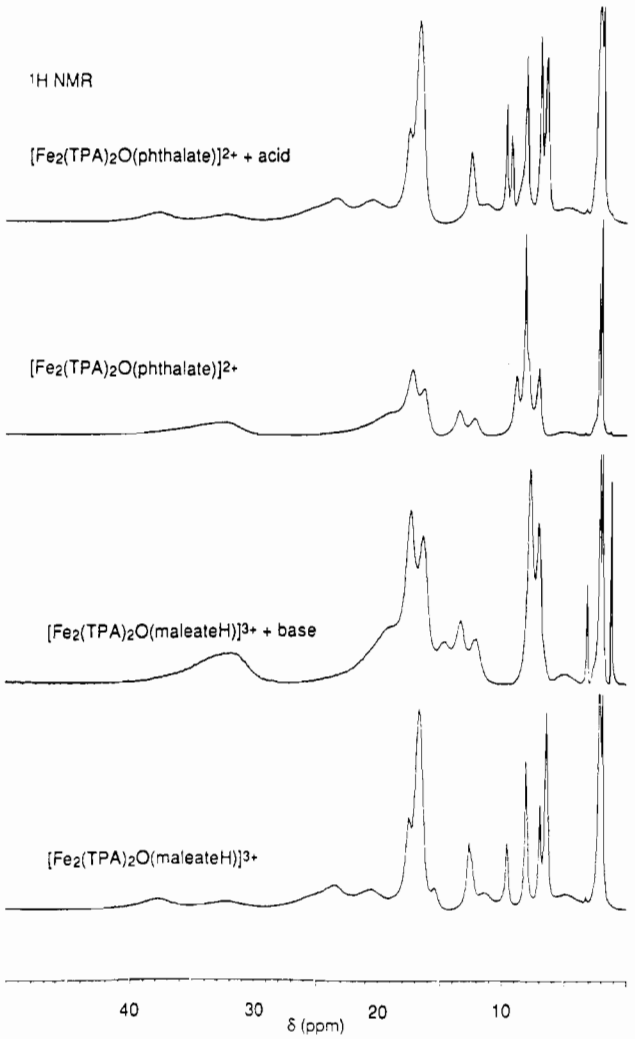

Figure 4. ^{1}H NMR spectra: (a) $[Fe_2(TPA)_2O(maleateH)]^{3+}$; (b) $[Fe_2(TPA)_2O(maleate)]^{2+}$ = $[Fe_2(TPA)_2O(maleateH)]^{3+}$ + 1 equiv of triethylamine; (c) $[Fe_2(TPA)_2O(phthalate)]^{2+}$; (d) $[Fe_2(TPA)_2O(phthalateH)]^{3+}$ = $[Fe_2(TPA)_2O(phthalate)]^{2+}$ + 1 equiv of perchloric acid. All spectra were recorded in the solvent CD_3CN.

The NMR features of **5–7**, which contain $O_xP\{R\}_y$ bridging groups, exhibit the patterns expected for complexes of the type that lack a 2-fold symmetry about the Fe–O–Fe core. The resonances due to the phenyl groups of **5–7** occur at their expected diamagnetic chemical shifts of 7.3, 7.4, and 7.4, respectively. However, the chemical shifts of the TPA protons, in general, are

(33) Yan, S.; Que, L., Jr.; Taylor, L. F.; Anderson, O. P. *J. Am. Chem. Soc.* **1988**, *110*, 5222–5224.
(34) Gafford, B. G.; Holwerda, R. A.; Schugar, H. J.; Potenza, J. A. *Inorg. Chem.* **1988**, *27*, 1126–1128.

Table VII. Properties of $[Fe_2(TPA)_2O(L)](ClO_4)_x$ Complexes

param	1, L = CO_3	2, L = OAc[a]	3, L = OBz[a]	4, L = malH	5, L = $O_3P(OPh)$	6, L = O_2PPh_2	7, L = $O_2P(OPh)_2$[a]	8, L = mal	9, L = phthal	10, L = Cl_2
Structural Data										
r_{Fe-O}, Å	1.800 (5)	1.790 (5)	1.795 (5)	1.794 (6)			1.797 (3)		1.792 (5)	1.790 (1)
∠Fe–O–Fe, deg	125.4 (3)	129.7 (3)	129.2 (2)	131.0 (3)			138.1 (2)		143.4 (3)	180
Electronic Spectra										
λ_{max}, nm	335 (10)	332 (10)	328 (12)	330 (12)	322 (14)	324 (12)	322 (14)	324 (9.2)	326 (12)	315 (sh, 10)
(ε, mM^{-1} cm^{-1})	372 (7.6)	366 (sh)	368 (sh)	360 (6.8)	360 (7.7)	360 (sh)	360 (7.7)	372 (8)	368 (10)	380 (0.82)
	425 (sh)	425 (sh)	425 (sh)	425 (sh)	420 (sh)	420 (sh)	420 (sh)			
	450 (1.1)	458 (1.2)	460 (1.2)	460 (1.21)	446 (0.84)	446 (sh)	446 (0.85)			
		492 (1.0)	492 (1.0)	490 (1.05)	480 (0.66)	484 (0.66)	480 (0.66)	486 (0.42)	492 (0.48)	490 (sh)
	500 (1.0)	504 (0.94)	504 (0.98)	506 (0.97)	490 (sh)	496 (sh)	490 (sh)			
	535 (sh)	530 (sh)	530 (sh)	530 (sh)	518 (sh)	518 (sh)	518 (sh)			
	700 (0.15)	700 (0.14)	700 (0.16)	694 (0.18)	634 (0.15)	636 (0.16)	638 (0.15)	598 (0.19)	604 (0.19)	560 (sh, 0.14)
	980 (0.005)	1050 (0.009)	1050 (0.01)	1050 (0.012)	1000 (0.01)	1050 (0.008)	1050 (0.008)	930 (0.008)	930 (0.01)	1010 (0.007)
Magnetic Properties										
$-J$, cm^{-1}	108.4	114.3	118.6	119.9	110.6	107.4	101.1		110.0	109.7
TIP, cgs/mol	0.000 215	0.000 03	0.000 03	0.000 28	0.000 606	0.000 16	0.000 17		0.000 20	0.000 438
p, mol %	0.16	0.058	0.045	0.30	0.64	0.01	0.44		0.029	0.017
g	2.02	2.04	2.06	2.03	2.00	2.02	2.03		2.00	2.01

[a] Reference 12b.

shifted downfield compared to those of other TPA complexes with bridging carboxylate ligands.

For **9**, the ^1H NMR spectrum has fewer features relative to other TPA dimers, reflecting the greater symmetry of the TPA environments in these complexes. In the 6–9 ppm region there are four peaks of relative intensity 2:4:2:2, corresponding to a pair of phthalate ring protons, the 4-protons of pyridine rings cis to the oxo bridge, the other pair of phthalate ring protons, and the 4-protons of pyridine rings trans to the oxo-bridge, respectively. There are two large, broad features of comparable intensity in the 18–40 ppm region and, in the 10–18 ppm region, four features of relative intensity 4:4:2:2 assigned to the pyridine 3,5-protons, with the more intense peaks arising from the rings cis to the oxo bridge and the others arising from the rings trans to the oxo bridge.

Interconversion of 1,3- and 1,6-Bridged Species. UV–vis and ^1H NMR studies on **4** and **9** demonstrate that the 1,3- and 1,6-bridged species are interconvertible. The electronic spectrum of **4** (Figure 5) consists of intense features in the near-UV region and weaker but nevertheless fairly intense bands in the 400–550-nm region, and even weaker features in the 550–1000-nm region. This spectrum is very similar to those found for **2** and **3** (Table VII) reflecting the similarity of the structures of the three complexes and those of tribridged complexes such as the methemerythrin–X complexes,[7] $[Fe_2(HBpz_3)_2O(OAc)_2]$,[22c] $[Fe_2(Me_3tacn)_2O(OAc)_2]^{2+}$,[22b] and $[Fe_2(BPA)_2O(OAc)_2]^{2+}$.[12b]

Titration of **4** with an equivalent of base results in the conversion of the initial amber color to bright green (**8**) (Figure 5) and affords a set of electronic spectra with isosbestic points near 650, 540, 440, and 360 nm, with the final spectrum resembling that of **9**. The electronic spectral features of the (μ-oxo)diiron(III) unit thus blue shifts as the dicarboxylic acid ligand goes from a μ-1,3-bridge to a μ-1,6-bridge. Conversely, titration of **9** with 1 equiv of acid affords analogous spectral changes in reverse and yields a spectrum similar to those of other 1,3-bridged carboxylate complexes.

These electronic changes are paralleled by the changes observed in the ^1H NMR spectra. Upon addition of an equivalent of base, the NMR features of **4** decrease in number, and a spectrum similar to that for **9** is observed (Figure 4b). The maleate protons now appear as a single feature at 14.7 ppm. Conversely, addition of an equivalent of acid to **9** (Figure 4d) results in a ^1H NMR spectrum that is typical of those for the asymmetric TPA oxo-bridged dimers **1–7**. Additional peaks at 9.2 and 9.7 ppm are also observed along with changes in relative intensities and a slight broadening of the peak at 6.9 ppm. These three features are assigned to the four phthalate ring protons.

Effects of the Fe–O–Fe Angle on Magnetism and Electronic Spectra. We thus have a series of $[Fe_2(TPA)_2O(L)](ClO_4)_x$ complexes where the Fe–O–Fe angle varies from 125 to 180°, which enables us to raise questions regarding the angular dependence of the electronic spectral and magnetic properties of the Fe–O–Fe unit. The data for these various complexes are collected in Table VII.

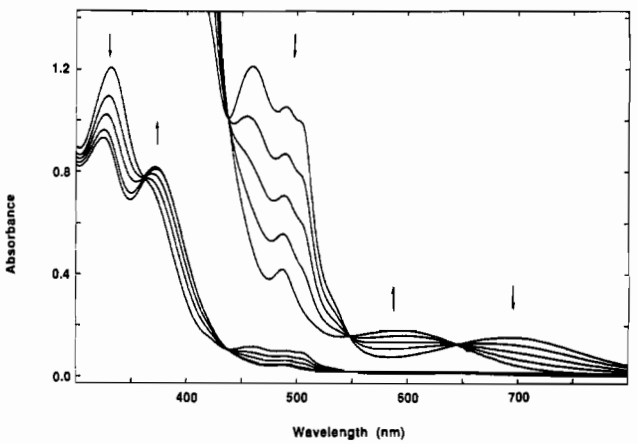

Figure 5. UV–vis spectral titration of $[Fe_2(TPA)_2O(maleateH)]^{3+}$ with triethylamine in CH_3CN (0.25 equiv of base added per succeeding trace). The spectra on the right have been magnified 10×. Data for the initial and final spectra are collected in Table VII.

Magnetic susceptibility measurements indicate that the J values for the TPA complexes range from -101 cm^{-1} for the diphenyl phosphate complex to -119 cm^{-1} for the 1,3-benzoate-bridged complex. As observed for the majority of (μ-oxo)diiron(III) complexes,[1,35] there does not appear to be any correlation between J and the Fe–O–Fe bridge angle over the range 125–180° in this series. These data are in contrast to the pairs of complexes studied by Murray[2] and Holm,[3] which suggested a dependence of J on the Fe–O–Fe angle. The lack of a correlation between J with the Fe–O–Fe angle in the TPA series supports the idea that multiple pathways for antiferromagnetic coupling are available for multielectron metal centers;[36] coupling via these pathways may maximize at different angles and thus result in the general insensitivity of J to the Fe–O–Fe angle.

The electronic spectra of these complexes, on the other hand, appear quite sensitive to structural variations (Figure 6). The bridging ligands vary in their basicity, charge, and bite angle and afford some insights into the nature of the observed electronic

(35) (a) Plowman, J. E.; Loehr, T. M.; Schauer, C. K.; Anderson, O. P. *Inorg. Chem.* **1984**, *23*, 3553–3559. (b) Thich, J. A.; Toby, B. H.; Powers, D. A.; Potenza, J. A.; Schugar, H. J. *Inorg. Chem.* **1981**, *20*, 3314–3317.

(36) Bossek, U.; Weyhermüller, T.; Wieghardt, K.; Bonvoisin, J.; Girerd, J. J. *J. Chem. Soc., Chem. Commun.* **1989**, 633–636.

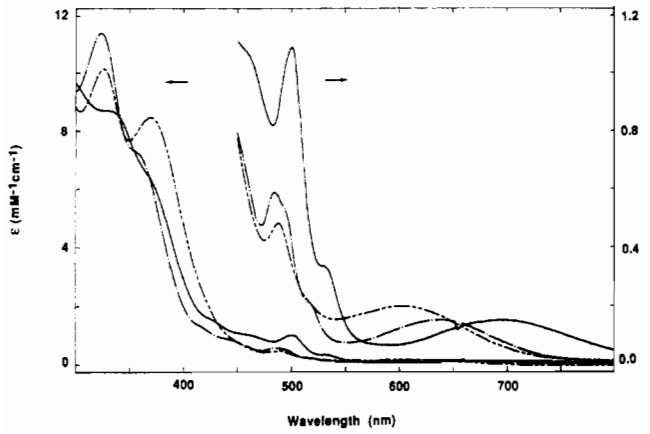

Figure 6. Visible spectra of **1** (—), **6** (-·-), and **9** (---) in CH_3CN.

transitions. The near-IR transitions at ca. 1000 nm (ϵ ca. 10 M^{-1} cm^{-1}) depend primarily on the charge of the bridging ligand and not on its bite angle. For example, the complexes with monoanionic bridges all have their near-IR bands near 1050 nm, despite the fact that the diphenyl phosphate bridge affords an Fe–O–Fe angle 8° larger than the carboxylate bridges. The four complexes with dianionic bridges, **1**, **5**, **8**, and **9**, have bands that are blue-shifted relative to 1050 nm, and the linear dichloride complex has a band at 1010 nm. The energies of the near-IR bands are thus affected by the ligand field strengths of the anionic ligands, consistent with Solomon's assignment[7] of this feature to the $^6A_1 \rightarrow {}^4T_1$ ligand field transition.

In contrast to the near-IR bands, the bands at 550–700 nm (ϵ ca. 150 M^{-1} cm^{-1}) appear to depend principally on the bite angle of the bridging ligand and are less sensitive to the ligand charge (Figure 6). The complexes that contain a μ-1,3-carboxylate bridge (**1**–**4**) all have bands near 700 nm, including the dianionic carbonate-bridged complex. The λ_{max} for this band shifts to near 640 nm for the complexes with PO_2 bridges (**5**–**7**) and further shifts to near 600 nm for the μ-1,6-maleate (**8**) and μ-1,6-phthalate (**9**) complexes. For the linear chloride complex, this band appears as a shoulder at 560 nm. The near-IR bands in these complexes vary just over 1000 cm^{-1} in energy, while the low-energy visible bands range over 3600 cm^{-1}. The Tanabe–Sugano diagram for a high-spin d^5 system shows that the two lowest energy transitions are expected to have very similar dependences on the strength of the ligand field, but our observations are inconsistent with these expected trends. Furthermore, the ligands order differently according to the energies of the two bands. For example, with respect to the near-IR band, that of the carbonate complex is blue-shifted relative to that of the diphenylphosphate complex. However, the order is reversed for the 550–700-mn band.

Spectral shifts similar to those found for the TPA complexes are observed for the bands in the 550–1100-nm region of the tribridged $[Fe_2L_2O(XO_2)_2]$ complexes (L = $HB(pz)_3$, Me_3tacn) when the bridges are systematically replaced (Table VIII). For the $HB(pz)_3$ series,[22c,23b] the $(PhO)_2PO_2$ and CH_3CO_2 complexes have near-IR bands of similar energy that are red-shifted relative to that of the Ph_2PO_2 complex, while in the 550–700-nm region the two complexes with μ-PO_2 bridges exhibit bands at similar energy, both of which are blue-shifted relative to that of the acetate complex. The more extensive Me_3tacn series also corroborates the trend observed for the 550–700-nm band.[22b,23c,24,37] There is a progressive blue shift as the bridge goes from $-CO_2$ to $-SO_2$ to $-PO_2$ and when S is replaced by Se and P by As; each of these can be rationalized by the increased bite of the bridging ligand and the consequent expansion of the Fe–O–Fe angle.

Our data together with those for the tribridged $HB(pz)_3$ and Me_3tacn complexes thus appear inconsistent with Solomon's assignment[7] that this feature is dominated by a $^6A_1 \rightarrow {}^4T_2$ ligand field transition. The expected $^6A_1 \rightarrow {}^4T_2$ ligand field transition likely occurs in the 550–700-nm region but is obscured by a more intense transition, the energy of which depends on the Fe–O–Fe angle. The transition most likely to be affected by the Fe–O–Fe angle is an oxo-to-Fe(III) charge-transfer transition. On the basis of the model proposed by Solomon,[7] such bands are expected to blue-shift as the Fe–O–Fe angle increases. The blue shift would arise from the increased π bonding between the iron atoms and the μ-oxo atom as the Fe–O–Fe angle approaches 180°. Such a bonding interaction decreases both the basicity of the oxo bridge and the Lewis acidity of the iron centers, thereby increasing the gap between the ligand donor and metal acceptor orbitals. Since the 550–700-nm band does appear to blue-shift as the Fe–O–Fe unit becomes linear, we assign this band to a forbidden oxo LMCT transition, which may gain intensity from mixing with the allowed LMCT bands at higher energy. Corresponding bands in the 550–700-nm region of the methemerythrin–X complexes presumably would be assigned similarly.

Table VIII. Comparison of Electronic Spectral Features of $[Fe_2L_2O(XO_2)_n]$ Complexes

L	μ-XO_2	∠Fe–O–Fe, deg	λ_{max}, nm (ϵ, mM^{-1} cm^{-1})	
TPA	CO_3^{2-}	125.4 (3)	700 (0.15)	980 (0.005)
	$CH_3CO_2^{-}$ [a]	129.2 (2)	700 (0.14)	1050 (0.009)
	$(PhO)_2PO_2^{-}$ [a]	138.1 (2)	638 (0.15)	1050 (0.008)
	$(PhO)PO_3^{2-}$		634 (0.15)	1000 (0.01)
	1,6-phthalate	143.4 (3)	604 (0.19)	930 (0.01)
$HB(pz)_3$	$CH_3CO_2^{-}$ [b]	123.6 (1)	695 (0.140)	995 (0.007)
	$Ph_2PO_2^{-}$ [c]	130.6 (2)	623 (0.120)	940 (0.007)
	$(PhO)_2PO_2^{-}$ [c]	134.7 (2)	625 (0.128)	1005 (0.009)
Me_3tacn	CO_3^{2-} [d]	113.8 (4)	677 (0.145)	990 (0.03)
	$CH_3CO_2^{-}$ [e]	119.7 (1)	729 (0.140)	1031 (0.007)
	SO_4^{2-} [f]	122.1 (5)	665 (0.170)	
	SO_3^{2-} [f]		660 (0.260)	
	SeO_3^{2-} [f]		634 (0.228)	
	$(PhO)PO_3^{2-}$ [g]	123.2 (3)	627 (0.190)	
	HPO_4^{2-} [g]		623 (0.196)	962 (0.005)
	$HAsO_4^{2-}$ [g]		614 (0.155)	

[a] Reference 12b. [b] Reference 22c. [c] Reference 23b. [d] Reference 24. [e] Reference 22b. [f] Reference 37. [g] Reference 23c.

The 400–550-nm region of the TPA series exhibits a number of features; the complexity of the region renders the effects of increasing the Fe–O–Fe angle more difficult to discern. However, close scrutiny of the spectral data (Table VIII; Figures 5 and 6) reveals that (a) the ca. 490-nm band is essentially independent of the Fe–O–Fe angle, while (b) the remaining features blue-shift and/or lose intensity as the Fe–O–Fe angle increases. In agreement with Solomon's assignment,[7] the ca. 490-nm band is the $^6A_1 \rightarrow ({}^4E, {}^4A_1)$ transition, the energy of which is expected to be independent of ligand field strength. Its intensity is presumably enhanced by borrowing from the oxo LMCT bands.

The other features in the 400–550-nm region are assigned to weak oxo LMCT transitions. The carboxylate complexes exhibit bands at ca. 460, 504, and 530 nm; these features shift to ca. 446, 480, and 518 nm in the μ-PO_2 complexes. On the basis of the same arguments we have employed for the 550–700-nm band, the blue shifts observed are consistent with the oxo LMCT assignment. However, these features become indiscernible in the phthalate and maleate complexes. It seems likely that the loss of intensity in the last two cases may be due to insufficient overlap between donor and acceptor orbitals engendered by the increase in the Fe–O–Fe angle.

The 300–400-nm region in the TPA series contains two bands of substantial intensity, which appear to have no systematic dependence on the Fe–O–Fe angle. They are likely to be allowed LMCT transitions but cannot be specifically assigned with the available data.

Conclusions

This series of (μ-oxo)diiron(III) complexes has afforded us the opportunity to assess the effects of the Fe–O–Fe angle on the spectroscopic and magnetic properties of complexes of this type. The magnetic data suggests that the Fe–O–Fe angle has little

(37) Wieghardt, K.; Drüeke, S.; Chaudhuri, P.; Flörke, U.; Haupt, H.-J.; Nuber, B.; Weiss, J. *Z Naturforsch.* **1989**, *44B*, 1093–1101.

effect on the magnitude of the coupling between the iron centers. The most pronounced angle dependence is observed in the visible spectra of these complexes; our studies suggest that many of these features are dominated by oxo-to-Fe(III) charge-transfer bands. These observations provide us with a better understanding of the spectral features found for (μ-oxo)diiron(III) centers in proteins.

Acknowledgment. We thank Professor J. D. Britton for his assistance and expertise with the structure determinations. This work was supported by grants from the National Institutes of Health (Grant No. GM-38767 to L.Q.) and the Louisiana Education Quality Support, administered by the Board of Regents of the State of Louisiana, and by the donors of the Petroleum Research Fund, administered by the American Chemical Society (C.J.O.). R.C.H. is grateful for a NIH postdoctoral fellowship (Grant GM-13919).

Supplementary Material Available: Ligand numbering scheme (Figure S1), tables of crystallographic parameters (Table S1), fractional atomic coordinates and isotropic thermal parameters (Tables S2–S4), bond lengths and angles (Tables S5–S7), and anisotropic thermal parameters (Tables S8–S10) for **1**, **4**, and **9**, and fits of the susceptibility data (Figures S2–S5) for **1**, **5**, **9**, and **10** (80 pages). Ordering information is given on any current masthead page.

Contribution from the Department of Chemistry,
Texas A&M University, College Station, Texas 77843

Solid-State and Solution Structure of (bpy)CuCo(CO)$_4$ (bpy = 2,2′-Bipyridine)

Donald J. Darensbourg,* Chi-Shan Chao, Christopher Bischoff, and Joseph H. Reibenspies

Received January 16, 1990

The heterobimetallic complex (bpy)CuCo(CO)$_4$ has been prepared by the reaction of NaCo(CO)$_4$ with 2,2′-bipyridine and CuCl in dichloromethane and has been characterized by X-ray crystallography at −80 °C. The complex crystallizes in the monoclinic space group $P2_1/a$, with unit cell dimensions a = 7.210 (3) Å, b = 16.580 (6) Å, c = 11.912 (6) Å, β = 97.88 (4)°, V = 1410 (1) Å^3, Z = 4, and R_F = 3.34%. The Cu–Co bond distance was found to be 2.404 (1) Å and to be supported by an asymmetrically bridged carbonyl ligand. This bridging CO group persists in polar solvents as well, as indicated by a ν(CO) band at 1850 cm^{-1} in the infrared spectra in both THF and Nujol mull. On the other hand, the Cu–Co bond is disrupted by a facile reaction at −78 °C with dppe (1,2-bis(diphenylphosphino)ethane) to provide the Co(CO)$_4^-$ anion and Cu(bpy)(dppe)$^+$.

Introduction

Although heterobimetallic complexes with transition metal to copper bonds are uncommon, the syntheses of dinuclear copper–cobalt derivatives originating from the reaction of the Co(CO)$_4^-$ anion and copper(I) salts have received some attention.[1,2] Because of the variety of CO bonding modes open in these derivatives, in particular the presence of semibridging carbonyls, it is of importance to assess their structures both in the solid state via X-ray crystallography and in solution by spectroscopic techniques. Indeed, the electronic structure and bonding in the derivative that has been structurally characterized, namely (tmed)CuCo(CO)$_4$ (tmed = tetramethylethylenediamine), have been described on the basis of Fenske–Hall molecular orbital computations.[3]

In relation to the studies indicated above, we have recently reported the synthesis and structure of [Cu(dmpe)$_2$][Cu(Co(CO)$_4$)$_2$], a complex containing copper(I) linearly bonded to two Co(CO)$_4^-$ anions.[4] Indeed, this latter complex was prepared in a manner completely analogous to that employed in the preparation of (tmed)CuCo(CO)$_4$ (eqs 1 and 2). At this time we wish

$$\text{CuCl} + \text{dmpe} + \text{NaCo(CO)}_4 \rightarrow \tfrac{1}{2}[\text{Cu(dmpe)}_2][\text{Cu(Co(CO)}_4)_2] + \text{NaCl} \quad (1)$$

$$\text{CuCl} + \text{tmed} + \text{NaCo(CO)}_4 \rightarrow \text{(tmed)CuCo(CO)}_4 + \text{NaCl} \quad (2)$$

to describe the solid-state and solution structure of (bpy)CuCo(CO)$_4$. This particular derivative was chosen for our investigation because it along with its 1,10-phenanthroline analogue had been suggested, on the basis of a complicated solid-state infrared spectrum, to contain a metal–carbonyl anion. Hence, it too might be formulated as [Cu(bpy)$_2$][Cu(Co(CO)$_4$)$_2$].

Experimental Section

Methods and Materials. All manipulations were carried out either in an argon drybox or on a double-manifold Schlenk vacuum line, using freshly distilled solvents. Reagent grade tetrahydrofuran and hexane were purified by distillation under nitrogen from sodium benzophenone ketyl. Dichloromethane was refluxed under nitrogen over phosphorus pentoxide and distilled prior to use. CuCl and 2,2′-bipyridine (bpy) were purchased from Aldrich Chemical Co. $Co_2(CO)_8$ and 1,2-bis(diphenylphosphino)ethane (dppe) were obtained from Strem Chemical Inc. NaCo(CO)$_4$ was prepared from NaOH and $Co_2(CO)_8$ according to published procedures.[5] Infrared spectra were recorded on an IBM FTIR/32 spectrometer.

Table I. Crystallographic Data for (bpy)CuCo(CO)$_4$

chem formula	$C_{14}H_8N_2O_4CoCu$	V, Å^3	1410 (1)
fw	390.7	Z	4
space group	$P2_1/a$	D_{calcd}, g/cm^3	1.840
a, Å	7.210 (3)	μ(Mo Kα), cm^{-1}	27.04
b, Å	16.580 (6)	λ, Å	0.71073
c, Å	11.912 (6)	R_F, %[a]	3.34
β, deg	97.88 (4)	R_{wF}, %[a]	3.22

[a] $R_F = \sum|\Delta|/\sum|F_o|$ and $R_{wF} = \sum(|\Delta|w^{1/2})/\sum(|F_o|w^{1/2})$, where $\Delta = |F_o| - |F_c|$.

Synthesis of (bpy)CuCo(CO)$_4$. CuCl (0.51 g, 5.2 mmol) was placed in a 100-mL Schlenk flask in the drybox. Upon removal of the flask from the drybox and the addition of 40 mL of CH_2Cl_2 by way of syringe, bpy (0.81 g, 5.2 mmol) in 30 mL of CH_2Cl_2 was added via cannula to the solution under N_2. The reaction was then placed under a CO atmosphere for 30 min. Subsequent to the addition of NaCo(CO)$_4$ (1.0 g, 5.2 mmol), the solution was stirred for 2 h and then filtered under N_2 to remove NaCl. The filtrate was concentrated to ca. 10 mL, and 60 mL of hexane was added. The product precipitated as an orange-red powder (1.5 g, 75%) and was recrystallized from CH_2Cl_2/hexane. Anal. Calcd for ($C_{14}H_8N_2O_4CoCu$): C, 43.01; H, 2.05. Found: C, 43.00; H, 2.05. IR (THF): 2024 (m), 1947 (vs), 1932 (s, sh), 1850 (m) cm^{-1}. IR (Nujol mull): 2020 (m), 1937 (vs), 1926 (s, sh), 1850 (m) cm^{-1}.

Reaction of (bpy)CuCo(CO)$_4$ with dppe. The complex (bpy)CuCo(CO)$_4$ was reacted with 1 equiv of dppe in THF at −78 °C. The reaction was monitored by IR spectroscopy, and the final infrared spectrum revealed formation of Co(CO)$_4^-$. The reaction rate of (bpy)CuCo(CO)$_4$ with incoming nucleophiles was dependent on the concentration and the nature of the nucleophile; e.g., dppe was found to react faster than PPh_3.

Reaction of (bpy)CuCo(CO)$_4$ with Water. Deoxygenated water was added to a flask containing a solid sample of (bpy)CuCo(CO)$_4$ under

(1) Hackett, P.; Manning, A. R. *J. Chem. Soc., Dalton Trans.* **1975**, 1606.
(2) Doyle, G.; Eriksen, K. A.; Van Engen, D. *Organometallics* **1985**, *4*, 877.
(3) Sargent, A. L.; Hall, M. B. *J. Am. Chem. Soc.* **1989**, *111*, 1563.
(4) Darensbourg, D. J.; Chao, C. S.; Reibenspies, J. H.; Bischoff, C. J. *Inorg. Chem.* **1990**, *29*, 2153.
(5) Edgell, W. F.; Lyford, J., IV. *Inorg. Chem.* **1970**, *9*, 1932.

0020-1669/90/1329-4637$02.50/0